In Situ Observations of Diurnal Variability in Rainfall over the Tropical Pacific and Atlantic Oceans[*]

Yolande L. Serra

JISAO, University of Washington, Seattle, Washington

Michael J. McPhaden

NOAA/Pacific Marine Environmental Laboratory, Seattle, Washington

ABSTRACT

In this study, the diurnal cycles in rain accumulation, intensity, and frequency are investigated for the 1997–2001 time period using measurements from self-siphoning rain gauges on moored buoys within the tropical Pacific and Atlantic Oceans. These measurements are unique in that they provide in situ, quantitative information on both the amplitude and phase of diurnal variability in tropical oceanic precipitation over an extended period of time at selected locations. Results indicate that the diurnal and semidiurnal harmonics explain a significant portion of the diurnal variance for all three rainfall parameters at the buoys. The diurnal harmonic in particular dominates the composite diurnal cycle in hourly rain accumulation, with a maximum from 0400 to 0700 local time (LT) and a minimum around 1800 LT. An early morning maximum and evening minimum are also observed in the composite diurnal cycles of rain intensity and frequency, indicating that both are contributing to the diurnal cycle in accumulation. Afternoon maxima in accumulation are also observed at several locations and are generally associated with maxima in rain intensity. While there is considerable variation in the estimates of the diurnal cycle both seasonally and regionally (especially for intensity), the results are overall consistent with previous studies of the diurnal cycle in rainfall and tropical cloudiness.

1. Introduction

Our ability to describe the diurnal cycle in rainfall is fundamental to understanding the processes that control convection in the Tropics.[1] The dependence of the stage of convection on time of day provides clues as to what constitutes a favorable environment for convective development and what processes are important at different points in the convective life cycle. The diurnal cycle in rainfall also influences the diurnal cycle in ocean mixing and thus upper-ocean heat and salt budgets. Short-term variability in surface temperature and rainfall inevitably affects satellite measurements, which must account for such variability in their measurement schemes (e.g., Trenberth et al. 2003). Numerical models also require

accurate rainfall measurements on short time and small space scales in order to validate convective parameterizations and ultimately improve model hydrological cycles (Yang and Slingo 2001).

Several studies of the diurnal cycle in tropical oceanic rainfall rely on indirect measurements of precipitation from satellites (e.g., Reed and Jaffe 1981; Albright et al. 1985; Janowiak et al. 1994; Chen and Houze 1997; Yang and Slingo 2001; Sorooshian et al. 2002; Nesbitt and Zipser 2003). While based on indirect observations of precipitation, these studies provide information about the diurnal cycle in rainfall over large areas and over open ocean regions not easily observed in situ. The collective result of these studies indicates that tropical open ocean cloudiness has a predawn maximum. An afternoon maximum in cloudiness is also observed in some regions such as the South Pacific convergence zone (SPCZ; Albright et al. 1985), the east Pacific ITCZ (Yang and Slingo 2001; Sorooshian et al. 2002) and the tropical Atlantic (Reed and Jaffe 1981; Yang and Slingo 2001). Janowiak et al. (1994) find that while deep clouds tend to peak in the predawn hours over tropical oceans, midlevel clouds peak in the afternoon. Similarly, Yang and Slingo (2001) also find that while there is a general trend for open ocean cloudiness to occur in the early-

[1] We define diurnal cycle to mean the variability in rainfall on all time scales up to 1 day.

Corresponding author address: Dr. Yolande Serra, JISAO, University of Washington, Box 357941, Seattle, WA 98195.
E-mail: yserra@u.washington.edu

morning hours, the phase of maximum cloudiness can be highly variable near coastlines and even over open ocean.

Surface observations of the diurnal cycle in oceanic rainfall are limited. Sui et al. (1997) use four months of data from surface radars collected for the Tropical Ocean Global Atmosphere Coupled Ocean–Atmosphere Response Experiment (TOGA COARE) to investigate the diurnal cycle in rainfall in the western tropical Pacific. Consistent with satellite studies such as those mentioned above, Sui et al. (1997) find that both stratiform and convective rainfall is maximum in the predawn hours. They also observe a secondary maximum in convective rainfall in the afternoon associated with less organized systems, in agreement with the Janowiak et al. (1994) satellite analysis. In another study, Gray and Jacobson (1977) use direct measurements of rainfall from island gauges in the Pacific for investigating the diurnal cycle in rainfall. They find that while the larger islands are subject to land heating effects resulting in an afternoon maximum in rainfall, the smaller islands are more consistent with other studies of tropical oceanic rainfall diurnal variability, exhibiting an early-morning maximum.

Janowiak et al. (1994) also observe an early-morning maximum in the frequency of rain when comparing their Tropics-wide satellite analysis to Comprehensive Ocean Atmosphere Data Set (COADS) observations of rain type collected by shipboard observers within the western tropical Pacific over a 10-yr period. They additionally observe an early-morning maximum in the frequency of heavy rain using measurements from five optical rain gauges on buoys in the west Pacific warm pool region deployed during TOGA COARE. Dai (2001) presents perhaps the most extensive study to date of surface precipitation data, using weather station data from land, island, and ocean stations, as well as shipboard data from COADS collected over a 22-yr period to examine the diurnal cycle in the frequency of rain over global land and ocean regions. This study also finds an early-morning maximum in the frequency of rain over open ocean for several types of rain. While collectively these studies have contributed greatly to our knowledge of in situ rainfall variability over a large portion of the globe, they either rely on a subjective classification system for observing rainfall (Janowiak et al. 1994; Dai 2001) or are fairly limited in time and space (Gray and Jacobson 1997; Janowiak et al. 1994; Sui et al. 1997).

In this study the diurnal cycle in rainfall is investigated using 1997–2001 measurements from self-siphoning rain gauges on Autonomous Temperature Line Acquisition System (ATLAS) buoys within the Tropical Atmosphere–Ocean/Triangle Trans-Ocean Buoy Network (TAO/TRITON) in the tropical Pacific and the Pilot Research Moored Array in the Tropical Atlantic (PIRATA) buoy arrays. Rainfall data from the East Pacific Investigation of Climate (EPIC) ATLAS buoys at 12°, 10° and 3.5°N along 95°W are also included in this study. The TAO/TRITON, EPIC, and PIRATA buoy arrays offer the first in situ quantitative measurements of tropical oceanic precipitation over an extended period of time in critical rain areas throughout the tropical Pacific and Atlantic Ocean basins. The spatial distribution of the buoys and their long time series allow us to organize the data into seven rainfall regions, from which we discuss both regional and seasonal characteristics of the diurnal cycles in rain accumulation, intensity, and frequency.

2. Buoy measurements

ATLAS buoys are designed and assembled at the National Oceanic and Atmospheric Administration/Pacific Marine Environmental Laboratory (NOAA/PMEL) for the TAO/TRITON and PIRATA arrays. Standard ATLAS measurements include 3-m air temperature and relative humidity, 4-m wind speed and direction, and ocean temperatures at 11 depths from 1 to 500 m. Next Generation ATLAS buoys, deployed for PIRATA and at selected locations in the Pacific since 1997, can also nominally measure shortwave radiation, precipitation, and salinity. Next Generation ATLAS buoys were deployed along 95°W in early 2001 as part of EPIC. Additional moorings at 12°, 10° and 3.5°N along 95°W were also deployed at this time as part of the EPIC long-term monitoring array and were recovered in the fall of 2003. Rainfall data from the Next Generation ATLAS buoys within the TAO/TRITON, EPIC, and PIRATA arrays collected from June 1997 to December 2001 are the focus of this study (Fig. 1).

The ATLAS buoys measure precipitation using self-siphoning rain gauges (R. M. Young Co.) mounted 3.5 m above the ocean surface. A complete description of the rain gauges used on ATLAS buoys and their error characteristics is given in Serra et al. (2001). Briefly, this study finds that the random error in hourly rain rates is on the order of 0.15 mm h^{-1}. While such accuracy is available from the ATLAS rain gauges, we have chosen to use a tolerance of 0.5 mm h^{-1}, or a value approximately halfway between R. M. Young Co.'s accuracy specifications of 1.0 mm h^{-1} and the threshold suggested by Serra et al. (2001) to calculate rain intensity and frequency. A threshold of 0.5 mm h^{-1} is also used by Yuter and Parker (2001) in their analysis of rainfall from these siphon gauges. Using a smaller threshold increases the average frequency of rain and decreases the average intensity over time periods longer than a day, but does not significantly affect the amplitude or phase of the diurnal cycle in these parameters. This is primarily due to the fact that rain rates less than 0.5 mm h^{-1} do not contribute to the diurnal cycle in the rainfall parameters, as indicated, for example, by the lack of a diurnal cycle in the frequency of light rain shown in Janowiak et al. (1994).

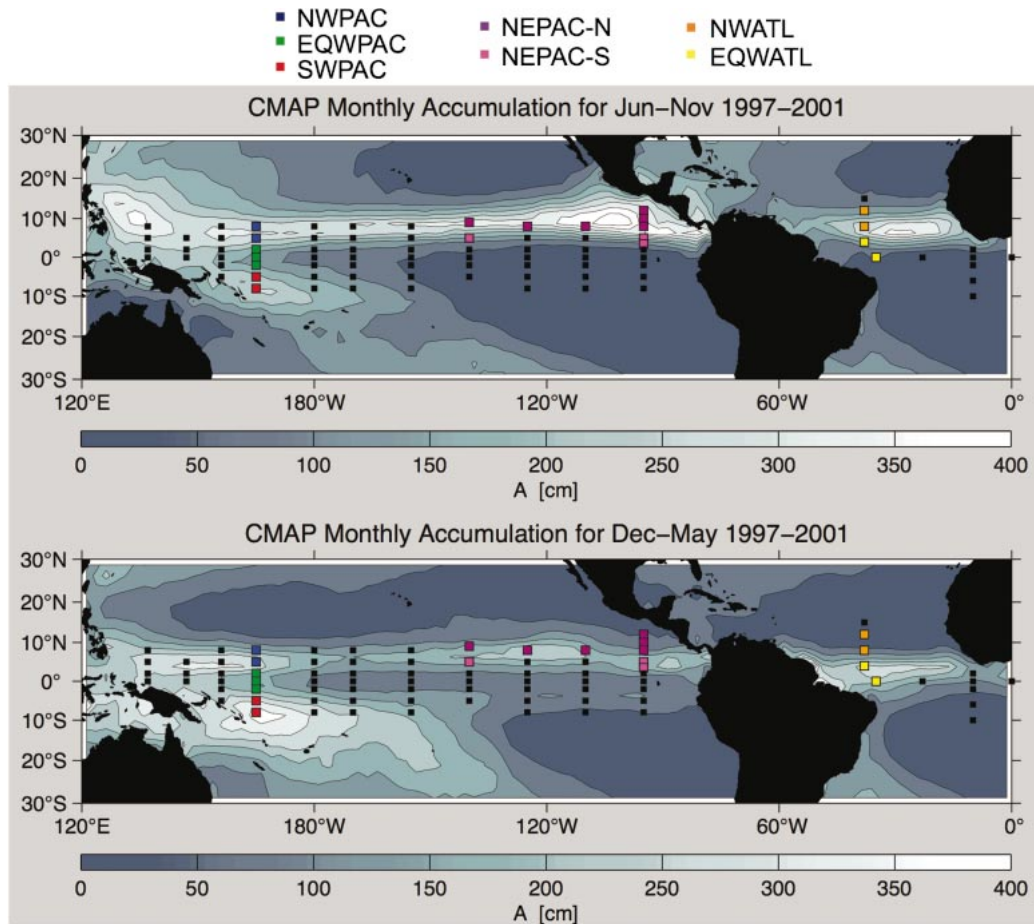The largest systematic error for siphon gauges is due

FIG. 1. TAO, EPIC, and PIRATA buoys overlaid on CMAP monthly rainfall for (a) Jun–Nov and (b) Dec–May.
Colored squares denote buoys within the seven rainfall regions used for this study.

to wind effects, which may bias the rain rates to be low by about 10%–50% for the wind speeds encountered at ATLAS buoys (Serra et al. 2001). A correction for this effect is provided in Serra et al. (2001) based on Koschmieder (1934). We have analyzed both the uncorrected and corrected buoy data for this study. In general, we find that the wind speed correction increases average rain intensity and frequency over time periods longer than a day but has little affect on the magnitude or phase of the diurnal cycle in these parameters. This is likely due to the fact that the amplitude of the diurnal cycle in wind speed is on the order of 0.2 m s^{-1} (Deser and Smith 1998). Wind speed anomalies of this magnitude would have little or no measurable effect on the undercatchment errors at the gauges. Because there is no wind speed correction available specific to the rain gauges used for this study and we are primarily interested in the diurnal cycle in the rainfall parameters rather than their long-term averages, we present the results for the uncorrected rainfall data. However, where long-term means are provided, both the uncorrected and corrected values are shown. The difference between the two in-

dicates the expected magnitude of wind-induced errors for our long-term mean calculations.

3. Methodology

a. Calculation of the diurnal cycle

ATLAS rain accumulation data are recorded at 1-min. intervals. These raw data are smoothed to hourly intervals using a 121-point (2 h) Hanning window. Smoothing with a 2-h Hanning window removes variability on time scales shorter than 1 h, thus these data nominally include variance at periods from 1-h to the record length. To get hourly rain rates or accumulations, the smoothed accumulation data are differenced over 1-h intervals, centered on the hour. We refer to these data as hourly accumulations or rainfall amount throughout the remainder of the text.

The frequency of rain events (F; in %) and their intensity (I; in mm h^{-1}) are related to rainfall accumulation (or amount, A; in mm) through the following equation:

$$A = (F/100) \times I \times \Delta T, \qquad (1)$$

where ΔT is the time interval. For the purposes of this study, ΔT will be 1 h, and (1) will apply to average diurnal cycles, unless otherwise noted. We define a rain event as any hour with an accumulation of greater than 0.5 mm. Thus, in the above equation rainfall frequency is the number of hourly accumulations greater than 0.5 mm divided by the total number of observations collected for a given local hour. These values are multiplied by 100 to get percent. Similarly, rainfall intensity in the above equation is the average of hourly accumulations greater than 0.5 mm for each local hour. By definition, rainfall frequency is a single number for any given hour and thus has no standard deviation associated with it. The 95% confidence limits for A and I are provided in the figures. Because there is only one local hour per day, each day of data is weighted equally for each parameter in (1).

As rain accumulation and intensity tend to be lognormally distributed, we define the composite diurnal cycle in these quantities using the lognormal mean and standard deviation of all hourly data for each local hour. Lognormal statistics place more weight on larger values to account for the fact that rainfall is a positive definite quantity and as a result has values concentrated near zero.

Block averaging the hourly data by local hour, as is done here, risks aliasing variability at lower frequencies into the calculation of the mean diurnal cycle. On the other hand, calculation of intensity and frequency is complicated if high-passed accumulation time series are used. Our calculations show that the high-passed accumulations provide similar diurnal cycles as the unfiltered hourly data, suggesting that aliasing is not a significant issue for this calculation.

The amplitude and phase of the diurnal and semidiurnal harmonics of the diurnal cycles in the rainfall parameters are found by fitting the mean diurnal cycles to the following equation,

$$\begin{aligned}
\overline{S} + S &= \overline{S} + S_1(\omega_1 t) + S(\omega_2 t) \\
&= \overline{S} + (b_1 \cos\omega_1 t + c_1 \sin\omega_1 t) \\
&\quad + (b_2 \cos\omega_2 t + c_2 \sin\omega_2 t), \qquad (2)
\end{aligned}$$

where $t = 1, 2, 3, \ldots, 24$. In the above equation $\omega_1 = 2\pi/24$, $\omega_2 = 2\pi/12$, S_1 and S_2 are the amplitudes of the diurnal and semidiurnal harmonics, respectively, and S is their sum. The mean value $\overline{S}$ of the rainfall parameters is also included in (2). We determine the relative significance of the diurnal and semidiurnal harmonics for the rainfall parameters by calculating the diurnal variance explained by S_1, S_2, and S.

b. Classification of the data into seven regions and two seasons

TAO/TRITON, EPIC, and PIRATA buoy locations are overlaid on the Climate Prediction Center (CPC) Merged Analysis of Precipitation (CMAP) rainfall (Xie and Arkin 1997) averaged for June–November (J–N) and December–May (D–M) in Fig. 1, where CMAP seasonal means are based on the 1997–2001 time period. Because of gaps in the buoy rainfall data, especially along 95°W, we choose to analyze the data using 6-month seasons rather than the more typical 3-month seasons. Similarly, we group the data into seven rainfall regions based on proximity and similarity in the seasonal cycle of rainfall. Serra and McPhaden (2003) show (December 1997–December 2001) time series of buoy monthly accumulations, along with Tropical Rainfall Measuring Mission (TRMM) and CMAP monthly accumulations, for a subset of the regions highlighted in Fig. 1. While there is some deviation at particular sites, in general buoys north of 5°N within the eastern Pacific and western Atlantic ITCZs have maximum monthly accumulations during J–N, while buoys at 3.5° and 5°N along 95°W and at 0°, 35°W and 4°N, 38°W in the southern portion of the ITCZ regions have maximum monthly accumulations during D–M (data not shown). The CMAP data shown in Fig. 1a support these results, indicating that during J–N the buoys at the northern extent of the ITCZ regions [north-northeast Pacific (NE-PAC-N), northwest Atlantic (NWATL)] receive most of the rainfall. This situation is reversed for D–M (Fig. 1b), when the buoys at the southern portion of the ITCZ regions receive most of the rainfall [south-northeast Pacific (NEPAC-S), equatorial western Atlantic (EQWATL)]. In contrast, little seasonal variation in rainfall is observed at the buoys in the northwest Pacific (NWPAC), equatorial west Pacific (EQWPAC), and southwest Pacific (SWPAC) regions in either the CMAP data shown in Fig. 1 or the buoy monthly accumulations shown in Serra and McPhaden (2003). The observed seasonality of rainfall at the buoys is also consistent with the results of Mitchell and Wallace (1992). Based on these results, we divide the rainfall data into two 6-month seasons and seven regions as defined in Fig. 1 to help with our interpretation of the data.

Table 1 lists the average number of days with rain (i.e., days with at least one hourly accumulation value >0.5 mm) and the average number of days with data for each buoy, as well as the totals for the composite dataset, where the average is based on the number of observations for each local hour. The composite data consist of nearly 1200 days of rain and nearly 19 000 days of data. The total number of days with rain and the total number of days with data for each region and for the J–N and D–M seasons are shown in Table 2. Composite seasons have over 1000 days of data, of which at least 70 are days with rain during rainy seasons.

It can be seen from the deployment dates in Table 1 that the time period for this study encompasses part of the 1997 El Niño and all of the 1998–2000 La Niña, making the data slightly biased toward cold conditions in the Tropics. The difference between the 1997–2001 averages shown in Fig. 1 and the long-term climatol-

TABLE 1. Rainfall data used for this study. Also see Fig. 1 for a map of buoy locations. Dates are given in yy-mm-dd format.

Region	Location	First deployment date	Last deployment date	No. of days with rain	No. of days with data
NWPAC	8°N, 165°E	97-06-10	01-12-31*	85	1000
	5°N, 165°E	97-06-11	01-12-31*	140	1503
EQWPAC	2°N, 165°E	98-01-07	01-12-31*	68	1275
	0°, 165°E	98-01-08	01-11-04	19	701
	2°S, 165°E	97-06-15	01-12-31*	48	931
SWPAC	5°S, 165°E	98-01-11	01-11-05	78	1033
	8°S, 165°E	97-06-17	01-12-31*	150	1683
NEPAC-N	9°N, 140°W	99-09-16	01-12-31*	88	846
	8°N, 125°W	97-10-04	98-05-66	14	234
	8°N, 110°W	97-08-22	98-10-22	29	309
	12°N, 95°W	00-11-12	01-12-31*	5	247
	10°N, 95°W	99-12-01	01-12-31*	15	698
	8°N, 95°W	97-08-05	01-12-31*	46	836
NEPAC-S	5°N, 140°W	98-05-14	01-12-31*	75	1470
	5°W, 95°W	99-05-26	01-11-23	55	796
	3.5°N, 95°W	99-11-29	01-11-24	26	722
NWATL	12°N, 38°W	99-02-03	01-01-06	26	1107
	8°N, 38°W	98-01-30	01-04-17	73	1253
EQWATL	4°N, 38°W	00-03-20	01-12-31*	58	777
	0°, 35°W	98-01-21	01-12-31*	80	1435
Total for the seven regions				1178	18 856

* Deployment extends beyond the end date shown, but only data through 31 Dec 2001 are used in this study.

ogies of CMAP rainfall (not shown) indicate that the warm pool and accompanying rainfall are shifted toward the west compared to "normal" for our data. These anomalies mainly affect the buoys along 165°E in the west Pacific. While the time series is too short to investigate the interannual variability in the diurnal cycle of rainfall, we do not expect that biases in our data due to predominant La Niña conditions would change the general nature of the findings reported herein.

4. Results

a. Composite diurnal cycles in the rainfall parameters

Figure 2 shows the composite diurnal cycle in hourly accumulation A, intensity I, and frequency F for all seven ocean regions combined. Also shown in this figure

TABLE 2. Number of days with rain and number of days with data by season for the seven regions defined in Fig. 1.

Region	No. of days with rain		No. of days with data	
	Jun–Nov	Dec–May	Jun–Nov	Dec–May
NWPAC	126	99	1420	1084
EQWPAC	71	65	1676	1232
SWPAC	91	137	1210	1506
NEPAC-N	145	51	1152	1952
NEPAC-S	36	120	1476	1513
NWATL	89	10	1092	1269
EQWATL	29	108	1038	1173

are the diurnal plus semidiurnal fits S to the diurnal cycles, where S is defined in (2). The horizontal line in each figure denotes the composite mean accumulation, intensity, or frequency symbolized by $\bar{S}$ in (2). The composite means are based on the total number of days with rain and days with data listed at the bottom of Table 1.

The composite diurnal cycle in accumulation has a broad maximum in the early morning from 0400 to 0700 local time (LT; Fig. 2a). There is also an indication of an increase around 1300–1500 LT, followed by the daily minimum at 1800 LT. The diurnal harmonic S_1 dominates the diurnal cycle in accumulation, explaining 78% of the mean variance in the composite diurnal cycle shown.[2] The composite diurnal cycle in intensity (Fig. 2b) is noisier than that of accumulation (95% confidence interval is several times that for A), but a similar early morning maximum is nevertheless discernible from 0400 to 0800 LT, as well as an evening minimum from around 1800 to 2000 LT. In addition, a secondary increase in intensity is also observed around 1300–1500 LT. The diurnal harmonic also dominates the mean diurnal cycle in intensity, but in this case only explains 52% of the observed variance of the combined data. Another 19% of the variance in intensity is explained by variability with an 8-h period (fit not shown), which captures the afternoon activity more prominent in intensity than in accumulation. Finally, the composite di-

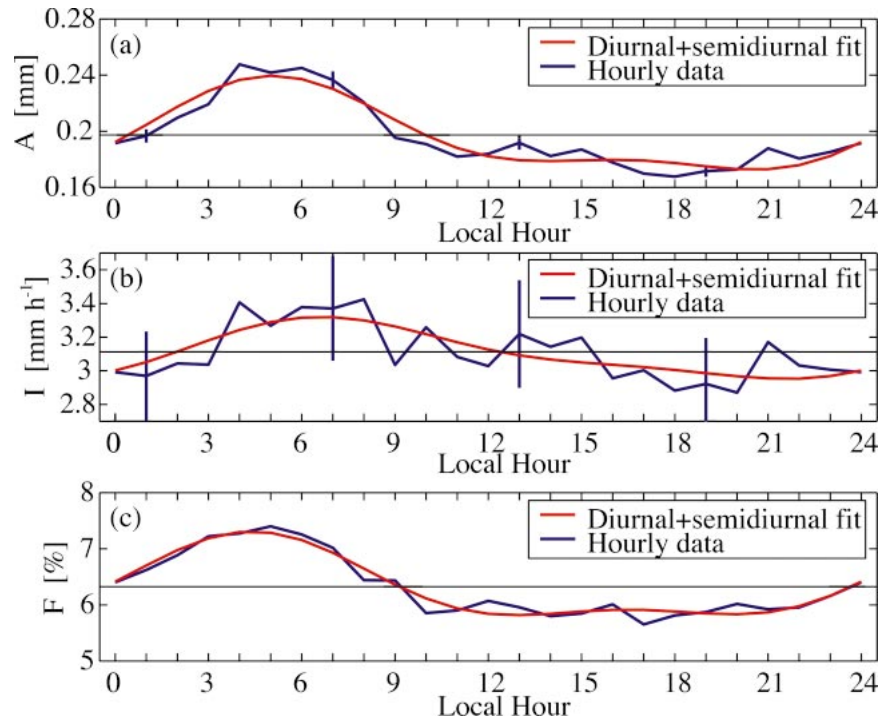[2] All r^2 values provided in the text are significant at the 95% confidence level unless otherwise noted.

FIG. 2. The composite diurnal cycle in (a) accumulation *A,* (b) intensity *I,* and (c) frequency *F.* The vertical lines in (a) and (b) indicate two standard errors of the mean, or the 95% confidence levels. Also shown are the diurnal plus semidiurnal fit to the data (red lines) and the long-term means (black lines).

urnal cycle in the frequency of rain has a single early-morning maximum from 0300 to 0600 LT and minimum values throughout the day and early evening (Fig. 2c). The diurnal harmonic again dominates the diurnal cycle, explaining 81% of the mean variance in frequency for the combined data.

Janowiak et al. (1994) show that the frequency of heavy rain (the upper 10% of their hourly rain accumulations) measured by optical rain gauges in the tropical west Pacific warm pool region has a larger diurnal amplitude than their medium or light rain categories. In addition, their analysis of the COADS precipitation data from 1970 to 1980 for the west Pacific warm pool region (10°N–10°S, 140°–160°E) also indicates that the frequency of heavy rain observations (showery precipitation and thunderstorm activity) has a larger diurnal

amplitude than that of the frequency of drizzle or nonshowery precipitation observations in the COADS data. In a more extensive analysis of COADS covering the period 1975–97, and using global ocean data, Dai (2001) also finds that the frequency of showery and nondrizzle precipitation observations have larger diurnal amplitudes over the global oceans than the frequency of drizzle observations. Comparing directly with the Janowiak et al. (1994) study, Sorooshian et al. (2002) also find that the frequency of heavy rain events over open ocean in the tropical west Pacific has a larger diurnal amplitude than the frequency of medium or light rain using rain rates derived from geostationary satellite infrared data corrected using Tropical Rainfall Measurement Mission (TRMM) microwave measurements.

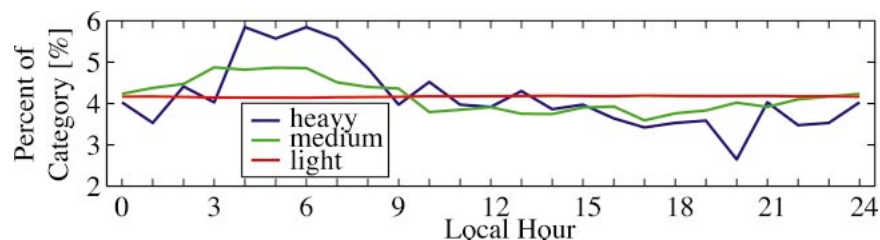Figure 3 shows the diurnal cycle in rainfall frequency

FIG. 3. Composite diurnal cycle in the frequency of rain for heavy, medium, and light categories. In this case, the frequency is normalized by the total number of observations in each category rather than the number of observations in each hour, as is done in Fig. 2c. See text for details.

from the TAO and PIRATA buoys for heavy, medium, and light categories following the method of Janowiak et al. (1994). As for Janowiak et al. (1994), the heavy rain category is defined as the upper 10% of our hourly rain events, the light rain category is defined as the number of rain events with 1 mm or less, and the medium category is everything in between. Also as in Janowiak et al. (1994), the values in the figure have been normalized by the total number of rain events in each category, rather than by the number of total observations for a given local hour, as was done in Fig. 2c.

The optical rain gauges discussed in Janowiak et al. (1994) are limited to a 1-mm resolution, with the lowest possible hourly accumulation being 1 mm. Thus, their light rain category differs slightly from ours, which includes hourly accumulations down to 0.5 mm. Nevertheless, we find that hourly rain events of 1 mm or less constitute approximately 31%–32% of the rain events in our data, similar to the 31.8% found by Janowiak et al. (1994) for the optical rain gauge data. On the other hand, the upper 10% of hourly accumulations for our data start at approximately 7.5 mm, nearly half of the value of the 14.6 mm defining the upper 10% of the optical gauge data. This difference is likely due to the fact that the optical rain gauge data in the Janowiak et al. (1994) study is limited to 4 months of data in the west Pacific warm pool region, while the TAO and PIRATA buoys represent a broader region and a longer time period.

Figure 3 shows that the results of Janowiak et al. (1994) apply to a broad area of the tropical oceans. The frequency of heavy rainfall has the largest diurnal cycle, peaking around 0400–0700 LT. The peak sharply drops off until about 0900 LT, at which time a steady 4% is observed until about 1500 LT, when a further decrease is seen in the frequency of events. The medium category has a smaller diurnal amplitude and peaks somewhat earlier than the heavy rate category, at approximately 0300–0600 LT. The light rain category has no discernible diurnal cycle. These results are in general agreement with Dai (2001), who also generalizes the results of Janowiak et al. (1994) to the global Tropics.

b. Regional and seasonal diurnal cycles in the rainfall parameters

The J–N and D–M diurnal cycles in accumulation are shown in Fig. 4 for the seven rain areas defined in Fig. 1. The vertical lines in these figures represent the 95% confidence limits, where each day has been weighted equally. As in Fig. 2, the diurnal plus semidiurnal fits to the data are also shown, indicating the magnitude and phase of these harmonics, as well as the degree to which the data are explained by these frequencies as a function of season and region. Figures 5 and 6 are the same as Fig. 4, but for intensity and frequency, respectively. As explained in section 3a, the frequency of rain at a given

hour has no standard deviation by our method of calculation.

The values of $\bar{S}$ from (2) in Figs. 4–6 for the diurnal plus semidiurnal fits are listed in Table 3 for each rainfall parameter and are based on the number of days of rain and days of data listed in Table 2. As for the diurnal cycle calculations, lognormal means and 95% confidence limits are shown for the accumulations and intensities listed in Table 3. The wind speed–corrected data (in parentheses) have higher average accumulations and intensities, since wind-induced errors bias rain rates to be low. Frequencies also increase by a few percent for the corrected dataset, as the number of hourly accumulations above the 0.5-mm threshold increases, adding to the count.

While we initially chose to separate the data into 6-month seasons in order to isolate the diurnal variability at locations with a strong seasonal cycle, comparing Figs. 4a and 4b, it is evident that even for locations where rainfall is relatively consistent over the 6-month periods, the diurnal variability shows significant differences between seasons. For instance, in the NWPAC during J–N there are two distinct maxima in rain accumulation: one in the early morning and one in the afternoon. However, during D–M at this location, there is a single early-morning maximum in rain accumulation and a minimum in the afternoon. In the SWPAC, the diurnal cycle during J–N is relatively flat, with the exception of a strong minimum in the early evening, indicating that rain is accumulating throughout most of the day. This can be compared to the diurnal cycle in accumulation during D–M in this region, which has a relatively large and prominent morning peak, as well as a small late-afternoon peak.

Seasonal and regional variability in the diurnal cycles in intensity (Fig. 5) and frequency (Fig. 6) are also observed in the west Pacific. As with the overall composite dataset, the diurnal variability in intensity tends to be on time scales of less than 12 h, while the diurnal variability in frequency is well described by the 24- and 12-h harmonics, S_1 and S_2. Also as with the composite dataset, diurnal variability in intensity is generally not highly significant based on the 95% confidence limits shown in Fig. 5. Despite this fact, there are instances in which the diurnal variability in intensity contributes significantly to the resulting diurnal variability in accumulation. For instance, in the NWPAC during J–N intensity tends to increase toward the afternoon and evening (Fig. 5a), while the frequency has a well-defined peak in the early morning, with a small secondary peak in the afternoon (Fig. 6a). The resulting diurnal cycle in accumulation has two equal amplitude peaks in the early morning and in the afternoon, as noted above.

The semidiurnal fit to accumulation in the NWPAC at this time has a slightly larger amplitude than the diurnal fit. In contrast, the diurnal amplitude in frequency is nearly double that of the semidiurnal ampli-
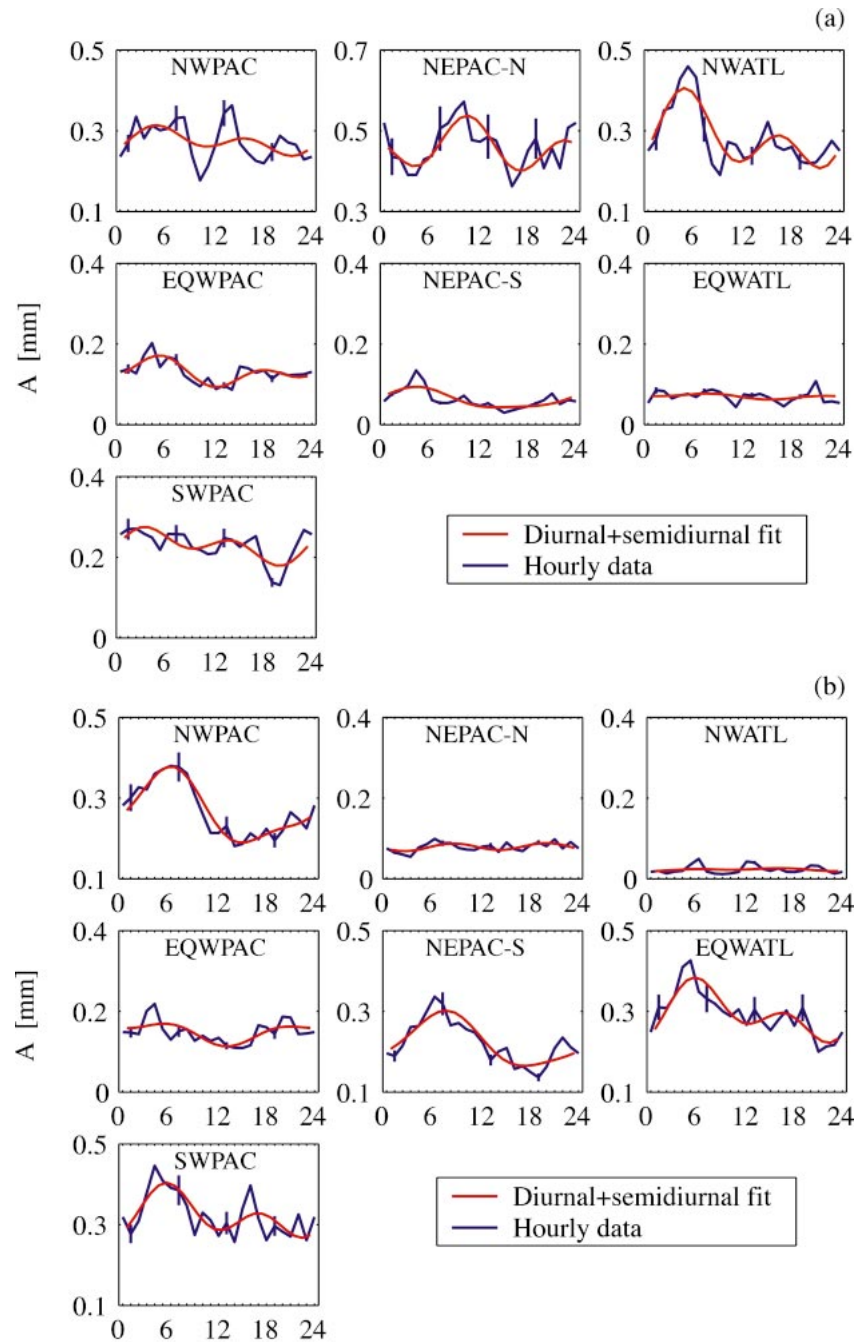
FIG. 4. The diurnal cycle in accumulation (blue lines) for the seven regions noted on the plots for (a) Jun–Nov and (b) Dec–May. The vertical lines indicate two standard deviations of the mean, or the 95% confidence levels. The sum of the diurnal and semidiurnal harmonics fit to the raw data are also shown (red lines). Times shown on horizontal axes are hours (local time).

tude for this case. Thus, while there is a great deal of uncertainty in the diurnal cycle in intensity, diurnal variations in this parameter appear to influence the more robust results found for the diurnal cycle in accumulation.

The apparent influence of intensity on accumulation

is again observed in the SWPAC where, similar to the NWPAC during J–N, afternoon accumulation in the SWPAC during D–M appears to result from relatively high afternoon intensities, with only a small corresponding peak in frequency at this time. The semidiurnal amplitude in accumulation in the SWPAC during D–M is
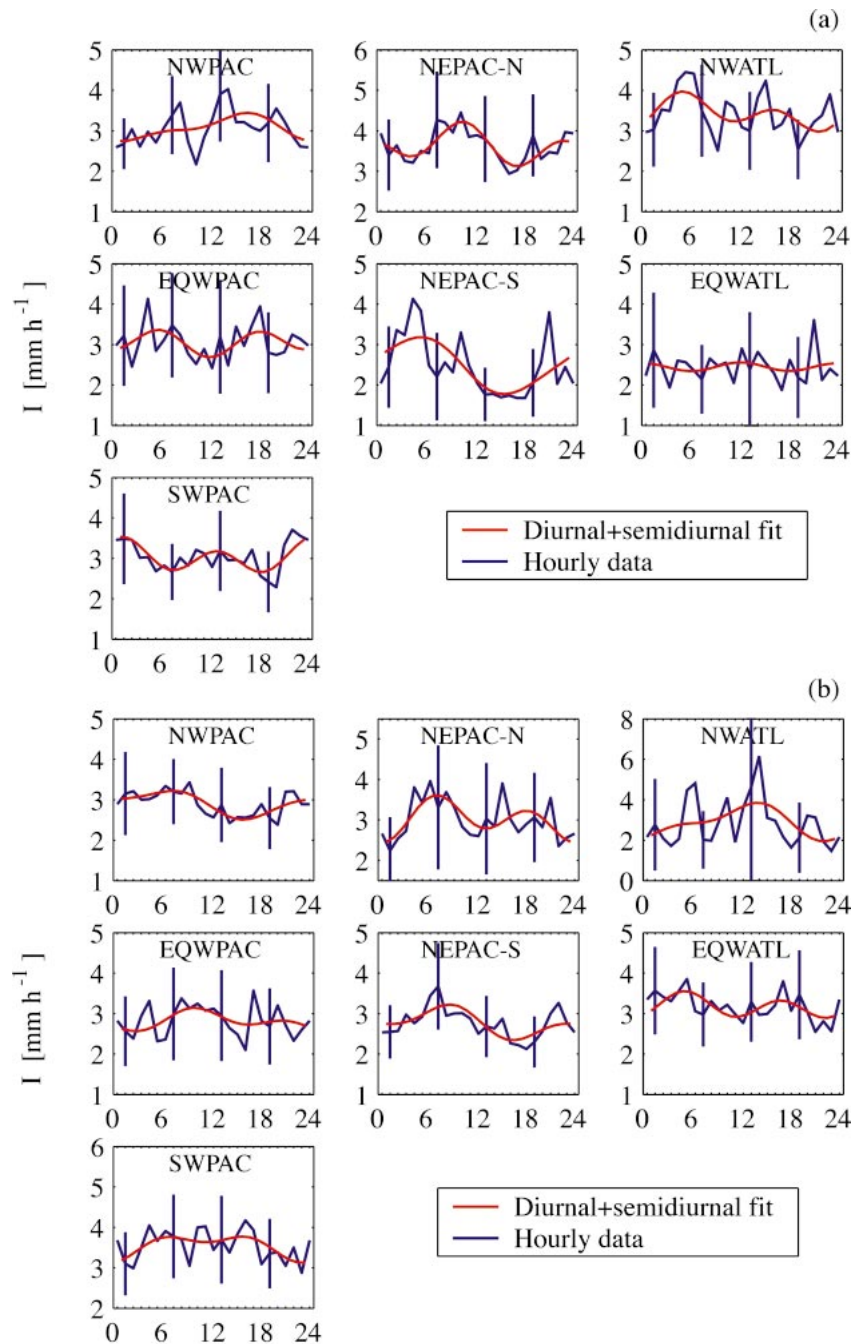
FIG. 5. As in Fig. 4, but for intensity.

slightly greater than the diurnal amplitude, with both fits significant at the 99% confidence level. In contrast, the diurnal amplitude in frequency is 50% larger than the semidiurnal amplitude, with both fits also significant at the 99% confidence level.

We can compare the results for the west Pacific diurnal cycle in rainfall parameters to those of Sorooshian et al. (2002), who find that, overall, the west Pacific has its maximum diurnal amplitude in hourly rain accu-

mulation during December–January–February (DJF). (They do not look at the semidiurnal harmonic). This is in agreement with our results, which indicate that the diurnal amplitude S_1 of all three rainfall parameters is larger for both the NWPAC and the SWPAC during D–M than during J–N. Previous studies also note an afternoon maximum in cloudiness in the SPCZ (Albright et al. 1985; Nesbitt and Zipser 2003). The late-afternoon peak in accumulation in the SWPAC during D–M, and
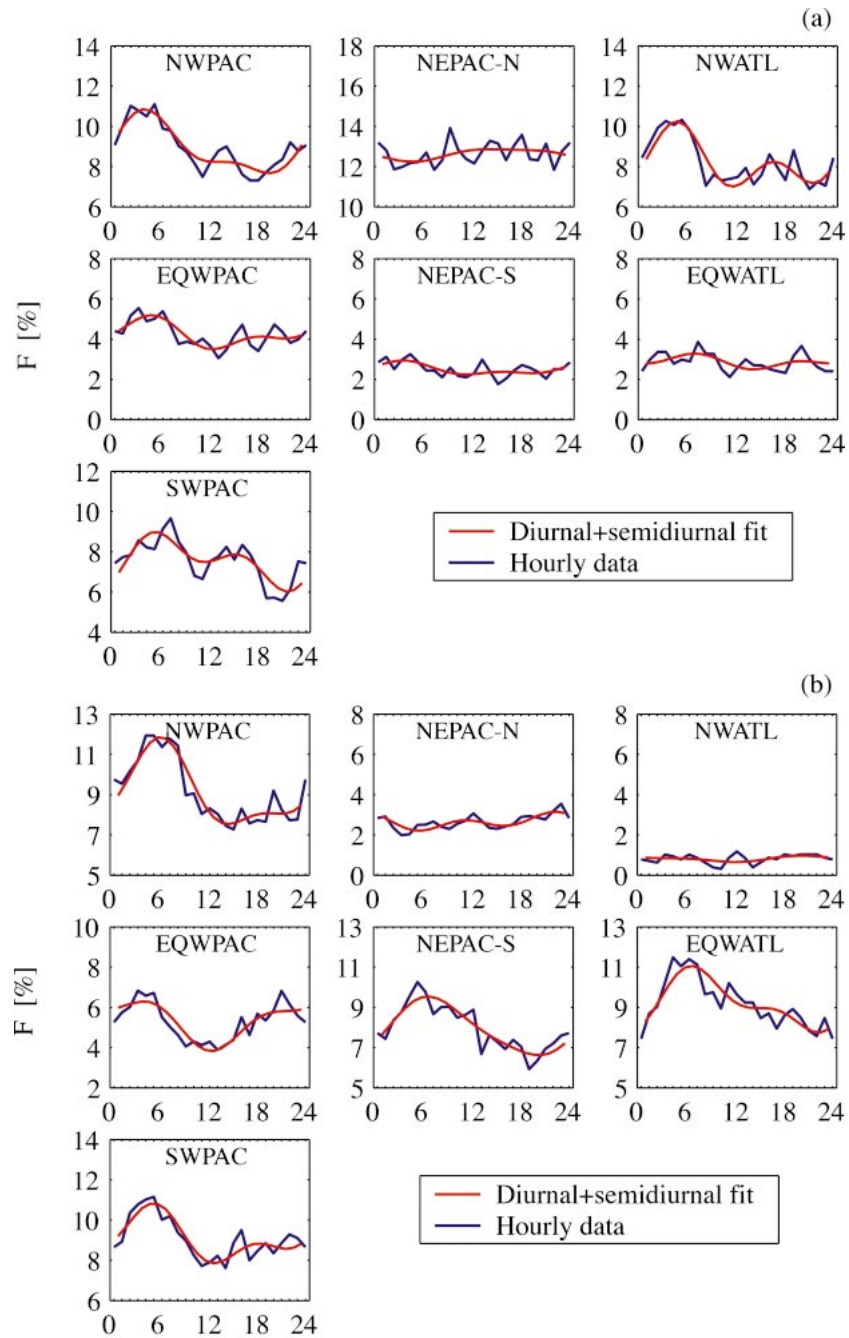
FIG. 6. As in Fig. 4, but for frequency. As there is only one value for each hour, no standard deviations are defined.

the afternoon peak in frequency for the SWPAC during J–N are consistent with these earlier results.

Considering only the rainy seasons in Figs. 4–6 when the rainfall statistics are most reliable, the northern and southern sections of the ITCZs also indicate significant regional differences in the amplitude and phase of the diurnal cycles in the rainfall parameters. The most striking example occurs in the NEPAC-N during J–N (Fig.

4a), where diurnal maxima in accumulation are observed in the late morning to early afternoon and at midnight, contrary to most other locations and regardless of season. These maxima are coincident with the diurnal maxima in rain intensity (Fig. 5a), while little significant diurnal variability in frequency is observed (Fig. 6a). Thus, the NEPAC-N provides another example of a case in which the diurnal cycle in rain ac

TABLE 3. The Jun–Nov and Dec–May seasonal mean accumulation (*A*), mean intensity (*I*), and frequency (*F*) for the seven regions defined in Fig. 1. Values based on wind speed–corrected rain rates are shown in parentheses. The 95% confidence limits are shown for *A* and *I*, assuming that each day is independent.

Region	Season	*A* (mm)	*I* (mm h^{-1})	*F* (%)
NWPAC	Jun–Nov	0.27 ± 0.02	3.0 ± 0.2	8.9
		(0.32 ± 0.03)	(3.3 ± 0.3)	(9.7)
	Dec–May	0.27 ± 0.02	2.9 ± 0.3	9.2
		(0.32 ± 0.03)	(3.3 ± 0.3)	(9.9)
EQWPAC	Jun–Nov	0.13 ± 0.01	3.0 ± 0.2	4.2
		(0.15 ± 0.01)	(3.2 ± 0.3)	(4.6)
	Dec–May	0.15 ± 0.01	2.8 ± 0.2	5.3
		(0.18 ± 0.02)	(3.2 ± 0.3)	(5.6)
SWPAC	Jun–Nov	0.23 ± 0.02	3.0 ± 0.3	7.6
		(0.28 ± 0.03)	(3.5 ± 0.3)	(8.1)
	Dec–May	0.32 ± 0.03	3.5 ± 0.3	9.1
		(0.39 ± 0.04)	(4.1 ± 0.4)	(9.5)
NEPAC-N	Jun–Nov	0.46 ± 0.04	3.6 ± 0.3	12.6
		(.57 ± 0.06)	(4.1 ± 0.5)	(13.8)
	Dec–May	0.078 ± 0.006	2.9 ± 0.2	2.6
		(0.103 ± 0.008)	(3.3 ± 0.3)	(3.1)
NEPAC-S	Jun–Nov	0.061 ± 0.004	2.4 ± 0.02	2.5
		(0.083 ± 0.008)	(2.7 ± 0.2)	(3.1)
	Dec–May	0.22 ± 0.02	2.8 ± 0.2	8.0
		(0.26 ± 0.02)	(3.0 ± 0.3)	(8.6)
NWATL	Jun–Nov	0.28 ± 0.03	3.4 ± 0.3	8.2
		(0.31 ± 0.04)	(3.7 ± 0.4)	(8.3)
	Dec–May	0.021 ± 0.002	2.6 ± 0.2	0.8
		(0.021 ± 0.002)	(2.9 ± 0.3)	(0.8)
EQWATL	Jun–Nov	0.069 ± 0.006	2.4 ± 0.2	2.9
		(0.088 ± 0.008)	(2.6 ± 0.2)	(3.3)
	Dec–May	0.29 ± 0.03	3.2 ± 0.3	9.3
		(0.32 ± 0.03)	(3.4 ± 0.3)	(9.5)

cumulation is strongly influenced by the diurnal cycle in rain intensity, despite the large standard deviations found for the diurnal cycle in intensity.

We took a closer look at the J–N diurnal cycles in accumulation for the individual buoys contributing to the NEPAC-N results shown in Fig. 4a (data not shown). All but the 10°N, 95°W buoy indicate late-morning/ early-afternoon positive anomalies in accumulation. However, some locations also indicate positive anomalies in accumulation in the predawn hours (12°N, 95°W; 10°N, 95°W; 8°N, 125°W), while others have a minimum at this time and/or a maximum closer to midnight (9°N, 140°W; 8°N, 110°W; 8°N, 95°W). Thus, combining these locations has likely accentuated the amplitude of the afternoon accumulation maximum relative to the night-time/predawn maxima due to phase differences in the latter. Nevertheless, afternoon accumulation is a significant signal in these data at several locations within the NEPAC-N region.

The results for the northeast Pacific ITCZ are in general agreement with Sorooshian et al. (2002), who observe a strong diurnal cycle in hourly rain accumulation in the Gulf of Tehuantepec (14°N, 95°W) from about June to October with a broad accumulation maximum from around midnight to 1200 LT. Their results also indicate an afternoon maximum in rain accumulation for these same months at 13°N, 100°W and a maximum

diurnal amplitude from April to August near 10°N, 100°W, with a maximum rain accumulation occurring in the early afternoon at this location. Yang and Slingo (2001) also find that this region has variability in the phase and amplitude of the diurnal cycle in rain accumulation over short spatial scales, and both Sorooshian et al. (2002) and Yang and Slingo (2001) note the influence of the land on the diurnal variability close to the coastline in this region. However, it is unlikely that such interactions would effect our data at 9°N, 140°W, where a significant late-morning to early-afternoon maximum in accumulation is also observed.

The remaining ITCZ regions—the NEPAC-S, NWATL, and EQWATL—all indicate early-morning maxima in accumulation during their respective rainy seasons (Fig. 4). Additional late-afternoon to early-evening activity is observed in the NWATL, and to some extent the EQWATL. Analysis of two years of satellite data within the Global Atmosphere Research Programme (GARP) Atlantic Tropical Experiment (GATE) region also indicates an afternoon maximum in hourly accumulation in the Atlantic ITCZ (e.g., Reed and Jaffe 1981). Similar to the far east Pacific, the afternoon maxima in cloudiness and hourly rain accumulation in the GATE region are attributed to land influences. However, as our buoys within the NWATL and EQWATL are west of this region, it is again unclear to what extent the two results can be compared.

c. Regional and seasonal significance of the diurnal and semidiurnal harmonics

In order to quantify the relative significance of the diurnal and semidiurnal harmonics in the buoy rainfall data, we first compare the amount of variance present in a subset of the data on subdaily time scales to the total variance over roughly a 6-month time period. Figure 7 shows an example of a power spectrum in hourly accumulations from 5°N, 165°E. The power spectrum is multiplied by frequency so that the area under the curve reflects the variance at each frequency. Also shown is the Ogive function (red line), defined as the cumulative sum of the power spectrum from high to low frequencies.

The Ogive function levels off at about 10 days, indicating that variance in hourly rainfall is contained primarily on time periods of 10 days or less. The variance in the hourly data over time periods of up to 1 day is 59% of the total variance over 180 days for these data. Performing a similar analysis on one buoy from each region using a continuous segment of data at least 120 days in length and with at least 450 mm of rain, we find that the variance on time periods of up to 1 day accounts for anywhere from 45%–60% of the roughly 6-month total variance in hourly rainfall at the selected buoys. Using satellite brightness temperature data, Yang and Sling (2001) find that variability on time periods of up to 1 day only accounts for 15%–20% of the total
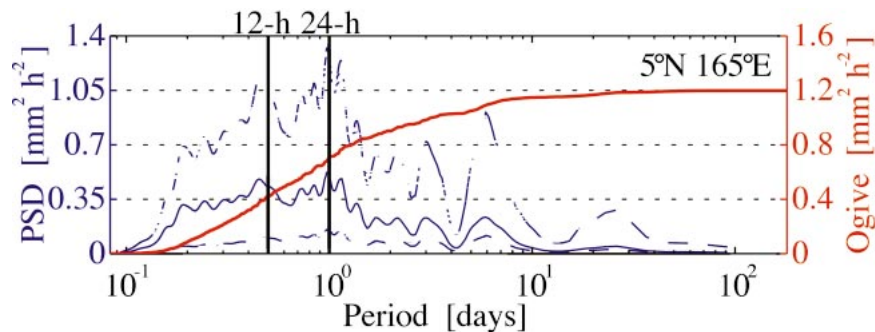
FIG. 7. The power spectrum and Ogive function for a 180-day time period of hourly accumulations at 5°N, 165°E.

variance in their data. As cloudiness tends to vary more slowly than hourly rainfall and their results are based on 3-hourly data, this discrepancy is not surprising.

We also quantify the fraction of variance for periods of up to 1 day, or diurnal variance, explained by the semidiurnal and diurnal harmonics for each rainfall parameter and for each region and season, in order to determine the significance of these harmonics on subdaily time scales. On a regional average, the diurnal and semidiurnal harmonics together explain 50% (57%) of the J–N (D–M) variance in A, 36% (40%) of the J–N (D–M) variance in $I,$ and 55% (70%) of the J–N (D–M) variance in F. The diurnal harmonic alone explains 27% (39%) of the J–N (D–M) variance in A, 17% (25%) of the J–N (D–M) variance in $I,$ and 37% (55%) of the J–N (D–M) diurnal variance in F. The semidiurnal harmonic alone explains 24% (18%) of the J–N (D–M) diurnal variance in $A,$ 19% (15%) of the J–N (D–M) diurnal variance in $I,$ and 17% (15%) of the J–N (D–M) diurnal variance in F.

The regional average values suggest that a slightly larger fraction of the daily variance is explained by the semidiurnal harmonic for J–N than for D–M for all three rainfall parameters. A closer look at each region reveals that for locations farthest north of the equator (NWPAC, NEPAC-N, and NWATL), the semidiurnal harmonic in accumulation and frequency explains more of the diurnal variance in these quantities and with greater significance for J–N (summer) than for D–M (winter). For intensity, only one of the three northern regions has at least 95% significance associated with the semidiurnal fit for D–M, while two have at least 95% significance associated with the semidiurnal fit for J–N. These results can be compared to the one region south of the equator (SWPAC), where more variance in accumulation is explained by the semidiurnal harmonic for D–M (summer) than for J–N (winter). On the other hand, the semidiurnal variance in frequency is similar to that of J–N for this region, while the semidiurnal variance in intensity is greater for J–N. These results suggest that within about 10° of the equator, afternoon rainfall is more likely in the summer than in the winter in the Northern Hemisphere (or northern branch of the ITCZ), while it is

perhaps equally as likely in either season in the Southern Hemisphere (or SPCZ). In addition, the diurnal and semidiurnal harmonics tend to explain a similar amount of the diurnal variance in intensity, while variance in frequency tends to be explained primarily by the diurnal harmonic alone. This latter result is consistent with Figs. 4–6 and suggests that afternoon and early-evening maxima in accumulation are generally associated with maxima in intensity, while early-morning maxima in accumulation are generally associated with maxima in frequency and intensity.

Our squared correlations for the diurnal variance in frequency are in general agreement with Dai (2001), who finds that the diurnal harmonic explains 40% of the mean daily variance in the frequency of occurrence of all precipitation types over the ocean in the COADS data. However, Dai (2001) does not find a seasonal dependence in the variance explained by the diurnal harmonic using 3-month seasons. There is considerable regional variability in the diurnal harmonic according to both datasets, and the buoys represent a more limited spatial domain than the COADS dataset. Thus, it is not surprising that our results differ to some extent. Differences may also be related to the different nature of the two measures of rainfall frequency, the COADS data being based on observers, and the buoy data being based on direct measurements.

Semidiurnal variability in rain intensity is noted by Sui et al. (1997) using radar data from TOGA COARE. Their mean areal average rain intensity over all 4-months of data indicates a single early-morning maximum around 0300 LT. When separated into convective and stratiform rain categories, however, they find that convective rain intensities have both an early-morning and afternoon maximum, while stratiform rain has a single early-morning maximum around 0300 LT. If their data are further divided into convectively active and suppressed conditions, mean rain intensity is seen to peak in the early morning during the active phase and in the afternoon during the suppressed phase. Janowiak et al. (1994) and Nesbitt and Zipser (2003) also find that afternoon convection is typically less extensive and shallower than early-morning systems. Thus, afternoon

and early-evening peaks in rain intensity at the buoys likely represent scattered and/or immature convective cells.

Contrary to the results from the buoys and Sui et al. (1997), Nesbitt and Zipser (2003) do not observe significant diurnal variability in rain intensity in the TRMM precipitation radar (PR) data averaged over the tropical oceans from 1997 to 2001. This discrepancy may result from sampling issues. The present study uses hourly data collected over a similar time period as the Nesbitt and Zipser (2003) data but only represent discrete points in space. The TRMM PR data, on the other hand, have roughly a 0.5–2-day time resolution, but have complete spatial coverage of the Tropics. Some studies have raised doubts that the PR sampling is sufficient for resolving the diurnal cycle in rainfall, even using 3 yr of data (Negri et al. 2002). In addition, Serra and Mc-Phaden (2003) attribute negative biases in the PR rain rates when compared to the buoys to sampling errors. As the Nesbitt and Zipser (2003) study does detect early-morning and afternoon convection with similar cloud properties and areal extents as those described by Sui et al. (1997) and Chen and Houze (1997), it is possible that while the structure of the convection described by the PR data is correct, the average rain rates may be subject to large sampling errors.

5. Summary and discussion

The composite diurnal cycle in accumulation at the buoys has a maximum from 0400 to 0700 LT and a minimum around 1800 LT. Afternoon maxima in accumulation are also observed in the NWPAC, NEPAC-N, and NWATL during J–N and in the SWPAC during D–M. The early-morning maximum in accumulation is coincident with a maximum in rain intensity and frequency, while afternoon maxima in accumulation observed at specific locations are most often associated with maxima in rain intensity.

The buoy data suggest that variability on time periods of an hour to one day comprises about half of the total variance in hourly rainfall over roughly a 6-month time period. Of this diurnal variance, anywhere from 5%–94% is explained by the diurnal and semidiurnal harmonics for the seasonal and regional data, or 78% for the data as a whole. The diurnal and semidiurnal harmonics explain about 4%–67% of the regional and seasonal diurnal variance in intensity, or 52% for the intensity data as a whole. Finally, 16%–90% of the regional and seasonal diurnal variance in frequency is explained by the diurnal and semidiurnal harmonics, or 81% for the data as a whole. Thus, the diurnal and semidiurnal harmonics are prominent in all three rainfall parameters but vary significantly with region and season.

Despite the large standard deviations of hourly means associated with the diurnal cycle in intensity for the composite data, as well as the regional and seasonal

data, diurnal variations in rain intensity are found to significantly contribute to the diurnal variations in rain accumulation at the buoys, especially in the afternoon. The seasonal and regional mean intensities for each local hour are typically based on less than 90 days of rain for the 4 yr of data included in this study. As the time period over which these data are available increases, the significance of the diurnal cycle in this quantity should be known with greater certainty. In the present study, we suggest that diurnal variability in intensity is important when diurnal variability in accumulation cannot be explained by frequency alone. We also attempt to place the results relating afternoon rain accumulation to variations in intensity in the context of previous studies (e.g., Nesbitt and Zipser 2003; Sui et al. 1997; Chen and Houze 1997; Janowiak et al. 1994), which suggest that the early-morning maximum in cloudiness/rainfall results from deep, organized convective systems, while the afternoon maximum in cloudiness/rainfall results from shallow, unorganized convection of limited areal extent. Thus, we conclude that afternoon and early-evening peaks in intensity at the buoys likely represent the observation of small, unorganized systems, while early-morning peaks in intensity and frequency likely represent the observation of deep, organized systems.

Overall, the TAO and PIRATA rainfall measurements are in general agreement with several previous satellite and in situ analyses of rainfall, placing confidence in these measurements as a whole. Our data, together with previous studies, suggest that there is a high degree of variability in the phase and amplitude of the diurnal and semidiurnal harmonics in all three rainfall parameters over open ocean in the Tropics. Processes related to the solar cycle that are thought to be important to convective development include radiation–cloud interactions (Gray and Jacobson 1977; Randall et al. 1991) and surface forcing (Chen and Houze 1997). There is also some suggestion that the diurnal pattern in low-level wind divergence, shown to be important to the diurnal cycle in rainfall over land (Dai et al. 1999), may also contribute to the diurnal cycle in rainfall over open ocean (Dai and Deser 1999; Dai 2001). More research is needed to understand specifically how these processes, and possibly others not yet discovered, produce the observed diurnal cycle in rainfall and its regional and seasonal variability.

REFERENCES

Albright, M. D., D. R. Mock, E. E. Recker, and R. J. Reed, 1985: The diurnal variation of deep convection and inferred precipitation in the central tropical Pacific during January–February 1979. *Mon. Wea. Rev.,* **113,** 1663–1680.

Chen, S. S., and R. A. Houze, 1997: Diurnal variation and life-cycle of deep convective systems over the Pacific warm pool. *Quart. J. Roy. Meteor. Soc.,* **123,** 357–388.

Dai, A., 2001: Global precipitation and thunderstorm frequencies. Part II: Diurnal variations. *J. Climate,* **14,** 1112–1128.

——, and C. Deser, 1999: Diurnal and semidiurnal tides in global surface wind and divergence fields. *J. Geophys. Res.,* **104,** 31 109–31 125.

——, F. Giorgi, and K. Trenberth, 1999: Observed and model-simulated diurnal cycles of precipitation over the contiguous United States. *J. Geophys. Res.,* **104,** 6377–6402.

Deser, C., and C. Smith, 1998: Diurnal and semidiurnal variations of the surface wind field over the tropical Pacific Ocean. *J. Climate,* **11,** 1730–1748.

Gray, W. M., and R. W. Jacobson, 1977: Diurnal variation of deep cumulus convection. *Mon. Wea. Rev.,* **105,** 1171–1188.

Janowiak, J. E., P. A. Arkin, and M. Morrissey, 1994: An estimation of the diurnal cycle in oceanic tropical rainfall using satellite and in situ data. *Mon. Wea. Rev.,* **122,** 2296–2311.

Koschmieder, H., 1934: Methods and results of definite rain measurements. *Mon. Wea. Rev.,* **62,** 5–7.

Mitchell, T. P., and J. M. Wallace, 1992: The annual cycle in equatorial convection and sea surface temperature. *J. Climate,* **5,** 1140–1156.

Negri, A., T. Bell, and L. Xu, 2002: Sampling of the diurnal cycle of precipitation using TRMM. *J. Atmos. Oceanic Technol.,* **19,** 1333–1344.

Nesbitt, S. W., and E. J. Zipser, 2003: The diurnal cycle of rainfall and convective intensity according to three years of TRMM measurements. *J. Climate,* **16,** 1456–1475.

Randall, D., Harshvardhan, and D. Dazlich, 1991: Diurnal variability of the hydrologic cycle in a general circulation model. *J. Atmos. Sci.,* **48,** 40–62.

Reed, R. J., and K. D. Jaffe, 1981: Diurnal variation of summer convection over West Africa and the tropical eastern Atlantic during 1974 and 1978. *Mon. Wea. Rev.,* **109,** 2527–2534.

Serra, Y. L., and M. J. McPhaden, 2003: Multiple time and space scale comparisons of ATLAS buoy rain gauge measurements to TRMM satellite precipitation measurements. *J. Appl. Meteor.,* **42,** 1045–1059.

——, P. A'Hearn, P. Freitag, and M. J. McPhaden, 2001: ATLAS self-siphoning rain gauge error estimates. *J. Atmos. Oceanic Technol.,* **18,** 1980–2001.

Sorooshian, S., X. Gao, K. Hsu, R. Maddox, Y. Hong, H. Gupta, and B. Imam, 2002: Diurnal variability of tropical rainfall retrieved from combined GOES and TRMM satellite information. *J. Climate,* **15,** 983–1001.

Sui, C.-H., K.-M. Lau, Y. N. Takayabu, and D. A. Short, 1997: Diurnal variations in tropical oceanic cumulus convection during TOGA COARE. *J. Atmos. Sci.,* **54,** 639–655.

Trenberth, K. E., A. Dai, R. M. Rasmussen, and D. B. Parsons, 2003: The changing character of precipitation. *Bull. Amer. Meteor. Soc.,* **84,** 1205–1217.

Xie, P., and P. A. Arkin, 1997: Global precipitation: A 17-year monthly analysis based on gauge observations, satellite estimates, and numerical model outputs. *Bull. Amer. Meteor. Soc.,* **78,** 2539–2558.

Yang, G.-Y., and J. Slingo, 2001: The diurnal cycle in the Tropics. *Mon. Wea. Rev.,* **129,** 784–801.

Yuter, S. E., and W. S. Parker, 2001: Rainfall measurements on ship revisited: The 1997 PACS TEPPS cruise. *J. Appl. Meteor.* **40,** 1003–1018.